Journal of Solid State Chemistry 181 (2008) 1992–1997

Contents lists available at ScienceDirect

Journal of Solid State Chemistry

journal homepage: www.elsevier.com/locate/jssc

Chemical equilibria involved in the oxygen-releasing step of manganese ferrite water-splitting thermochemical cycle

L. Seralessandri, M. Bellusci, C. Alvani, A. La Barbera, F. Padella, F. Varsano *

ENEA-C.R. Casaccia, Italian National Agency for New Technologies, Energy and the Environment, Via Anguillarese 301, 00123 Roma, Italy

ARTICLE INFO

Article history:
Received 19 December 2007
Received in revised form
10 April 2008
Accepted 12 April 2008
Available online 30 April 2008

Keywords:
Thermochemical water-splitting cycle
Hydrogen production
Manganese ferrite
Energy sustainability
XRD
Rietveld analysis
Na de-intercalation

ABSTRACT

Sodium ferrimanganite carbonatation reaction was investigated at different temperatures/carbon dioxide partial pressures to evaluate the feasibility of the thermochemical water-splitting cycle based on the $MnFe_2O_4/Na_2CO_3/Na(Mn_{1/3}Fe_{2/3})O_2$ system.

After thermal treatments in selected experimental conditions, the obtained powder samples were investigated by using the X-ray diffraction (XRD) technique and Rietveld analysis.

Two different lamellar $Na_{1-x}Mn_{1/3}Fe_{2/3}O_{2-\delta}$ phases were observed together with the expected $MnFe_2O_4/Na_2CO_3$ mixture. Different equilibrium regions among sodium-depleted lamellar phases, manganese ferrite and sodium carbonate were found as a function of the different reaction conditions. A hypothesis concerning the regeneration mechanism of the initial compounds is proposed. Chemical equilibrium between stoichiometric and sub-stoichiometric forms of sodium ferrimanganite and sodium carbonate formation/dissociation appears to be essential factors governing the oxygen-releasing step of the manganese ferrite thermochemical cycle.

1. Introduction

The manganese ferrite water-splitting thermochemical cycle [1,2] is a two-step process based on a $MnFe_2O_4/Na_2CO_3$ solid reactive mixture. The cycle consists of a sequence of two reactions that permits one to separately obtain hydrogen and oxygen from water as schematized by

$$2MnFe_2O_{4(s)} + 3Na_2CO_{3(s)} + H_2O_{(g)} \rightarrow 6Na(Mn_{1/3}Fe_{2/3})O_{2(s)} + 3CO_{2(g)} + H_{2(g)} \quad (1)$$

$$6Na(Mn_{1/3}Fe_{2/3})O_{2(s)} + 3CO_{2(g)} \rightarrow 2MnFe_2O_{4(s)} + 3Na_2CO_{3(s)} + 1/2O_{2(g)} \quad (2)$$

In reaction (1) hydrogen evolves from water as a consequence of the oxidation of Mn^{II} in the starting spinel to produce sodium ferrimanganite [3]. The following step (2) consists of a disproportion reaction induced by carbon dioxide. Oxidized Mn^{III} contained in the sodium mixed ferrite can be reduced to Mn^{II} so that the starting manganese ferrite is regenerated and oxygen release from the oxide crystalline network occurs. The two reactions can be alternately repeated so that when the system is coupled to a renewable energy source, such as a solar concentrator, sustainable hydrogen production is obtained.

From a technological point of view, when compared to other water-splitting thermochemical cycles [4–9], the manganese ferrite cycle appears to be a very promising hydrogen production system. In fact, due to the low temperature (700–800 °C) of both reactions [10–12] it appears relatively easy to implement in a real plant and a scaling-up without significant changes in conventional reactor design and materials can be hypothesized.

Although irreversible features in the oxygen-release step were initially supposed [13,14], in a recent analysis of the disproportion reaction (2) a T/P_{CO_2} diagram permitted one to define different phase equilibrium regions [12]. While for certain T/P_{CO_2} conditions some phases different from the expected ones were detected, a region of complete regeneration of the starting powder mixture was evidenced. In this region reacted powders were composed exclusively by the starting $MnFe_2O_4/Na_2CO_3$ mixture.

To investigate relationships among the several phases observed in the stability diagram [12], the compound mixtures obtained in the different regions were fully characterized by using the X-ray diffraction (XRD) technique. The Rietveld method was applied to collected patterns to characterize structures and chemical composition of the observed phases. Quantitative phase analysis (QPA) obtained from numerical elaboration was utilized as a chemical tool to obtain information on the possible path of the regenerative step.

* Corresponding author. Fax: +39 6 3048 4273.
E-mail address: francesca.varsano@casaccia.enea.it (F. Varsano).

0022-4596/$ - see front matter © 2008 Elsevier Inc. All rights reserved.
doi:10.1016/j.jssc.2008.04.014

2. Materials and methods

Solid chemicals (Fe_2O_3, $MnCO_3$ and Na_2CO_3) were supplied by Carlo Erba, analytical grade. Gaseous reactants (Ar, O_2, CO_2 and N_2/O_2 mixture) were supplied by Alpha Gaz, analytical grade.

Sodium ferrimanganite (to be exposed to CO_2 in selected p/T conditions) was obtained inside a Netzsch STA 409 thermobalance by thermal treatments of $MnFe_2O_4/Na_2CO_3$ mixture. The following experimental procedure was applied: (i) stoichiometric mixtures of $MnFe_2O_4$ and Na_2CO_3 were oxidized at 750 °C by fluxing Ar/O_2 40:10 gas mixture (50 cm^3/min) for 2 h; (ii) after Ar/O_2 flow is closed, residual O_2 was removed by Ar flow (50 cm^3/min) for 30 min at 750 °C; (iii) the resulting oxidized product was *in situ* exposed to different Ar/CO_2 mixtures (50 cm^3/min) at selected temperature values in 600–800 °C range. All samples were treated in isothermal conditions for 12 h, a time interval that is long enough for the sample to reach a weight stationary value.

Reacted powders were analyzed by XRD measurements. For this purpose powder samples were sealed in glass capillary tubes (0.1 mm diameter) to limit interactions with air during exposure to X-rays. All samples were analyzed by using a Siemens D500 apparatus equipped with Mo $K\alpha 1$ radiation ($\lambda = 0.07093$ nm) and a quartz monochromator on the incident beam. Diffraction data were collected in the angular range $4° < 2\theta < 40°$ with a 0.02° step size and 30 s collection time, exploring 6.183–60.594 nm^{-1} s ($= 4\pi\sin(\theta)/\lambda$) intervals.

For comparative purposes, a reference sodium ferrimanganite $NaMn_{1/3}Fe_{2/3}O_2$ sample was obtained by thermally activated solid-state reaction among $Fe_2O_3/MnCO_3/Na_2CO_3$ (1:1:1.5 by mole) mixture. A Lenton C2 tubular oven fluxed by N_2/O_2 gas was used for the purpose. The oven was heated with a 5 °C/min scan rate up to 1000 °C and then a 16 h isothermal step followed. After cooling, the powder was ground inside a mortar and the thermal procedure was repeated a second time. At the end of the procedure the sample was collected and stored inside an Ar-filled glove box. The reference sodium ferrimanganite $Na(Mn_{1/3}Fe_{2/3})O_2$ single-phase sample was measured using a high-intensity Seifert Pad VI diffractometer equipped with a LiF Johan monochromator on diffracted beam.

All obtained patterns were indexed by using the JCPDF-ICDD database [15], supposing an isostructural metal substitution in identified phases if required.

Crystallochemical information, as well as QPA were obtained by applying the Rietveld method [16,17] on collected patterns, by using General Structure Analysis System [18] software. If found, data contained in the ICSD database [19] were utilized as starting models. The refinement procedure was carried out respecting the metal ratio in the sodium ferrimanganite stoichiometry (Na:Mn:Fe = 3:1:2) and the goodness of obtained refinements were evaluated by using R_{wp} and R_p residual pattern indexes and the χ^2 factor [17].

3. Results and discussion

3.1. The P/T diagram and identified chemical compounds

Representative thermogravimetric curves are shown in Fig. 1 for different experimental conditions. All examined samples exhibit an abrupt weight increase immediately after exposure to CO_2, reaching different stationary values as a function of the selected experimental conditions. By analyzing powder compositions after thermal treatments, several solid phases arising from the $Na(Mn_{1/3}Fe_{2/3})O_2$ carbonatation process were observed. Three different regions with similar phase occurrence were identified [12] and are reported in Fig. 2. In the identified regions (labeled A, B and C), powders exhibit representative XRD patterns reported in Fig. 3. As evidenced by curve a in Fig. 3, powders in the A region are composed by a mixture of $MnFe_2O_4$ and Na_2CO_3 compounds (JCPDS card nos. 10-319 and 37-451 respectively). This region identifies the experimental conditions where the carbonatation of sodium ferrimanganite is able to completely regenerate the starting manganese ferrite/sodium carbonate mixture. Patterns b and c in Fig. 3 contain evidence of other phases, which correspond to two different sodium-depleted $Na_{1-x}(Mn_{1/3}Fe_{2/3})O_{2-\delta}$ and show different XRD features.

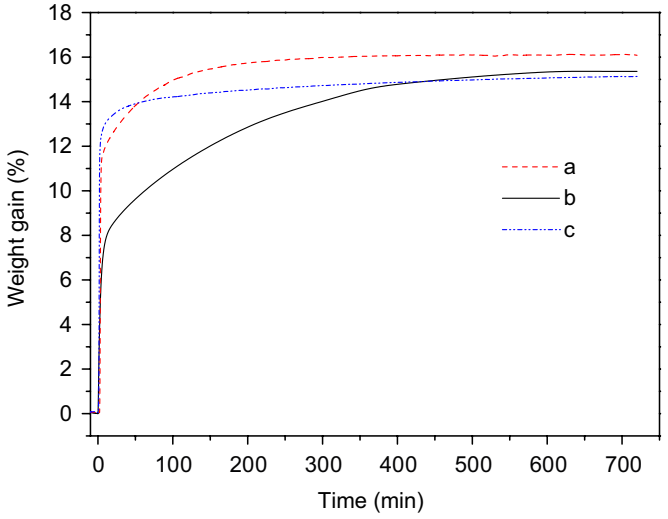

Fig. 1. Thermogravimetric analysis of sodium ferrimanganite $Na(Mn_{1/3}Fe_{2/3})O_2$ exposed to carbon dioxide during 12 h. (a) $P_{CO_2} = 0.8$ atm, $T = 750$ °C, (b) $P_{CO_2} = 0.5$ atm, $T = 750$ °C and (c) $P_{CO_2} = 0.8$ atm, $T = 600$ °C.

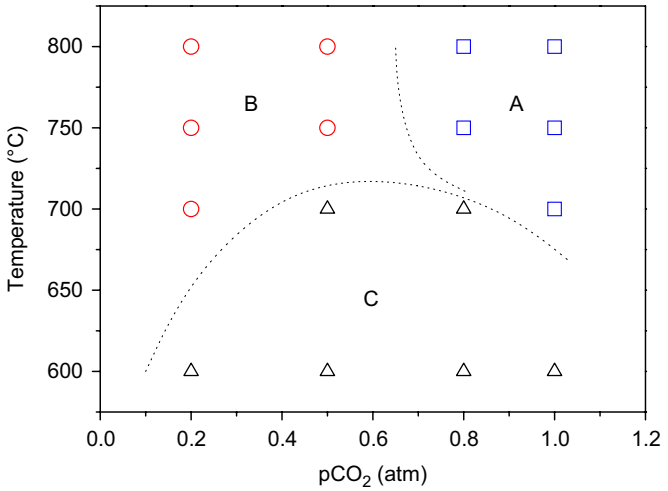

Fig. 2. Phase stability diagram of $Na(Mn_{1/3}Fe_{2/3})O_2/CO_2$ system. Labels A, B, C, in the T/P_{CO_2} diagram denote zones where powders show same phase occurrences in XRD patterns (□ = $MnFe_2O_4$, Na_2CO_3, ○ = O3–$Na_{1-x}Mn_{1/3}Fe_{2/3}O_{2-\delta}$, $MnFe_2O_4$, Na_2CO_3 and Δ = P3–$Na_{1-x}Mn_{1/3}Fe_{2/3}O_{2-\delta}$, $MnFe_2O_4$, Na_2CO_3). Dotted lines represent indicative boundaries among different stability fields.

3.2. The $Na(Mn_{1/3}Fe_{2/3})O_2$ compounds

Different $NaMn_{1/3}Fe_{2/3}O_2$ compounds found in diffractograms were fully investigated by applying the Rietveld analysis to collected patterns. In the following the main evidence resulting from the analysis is reported.

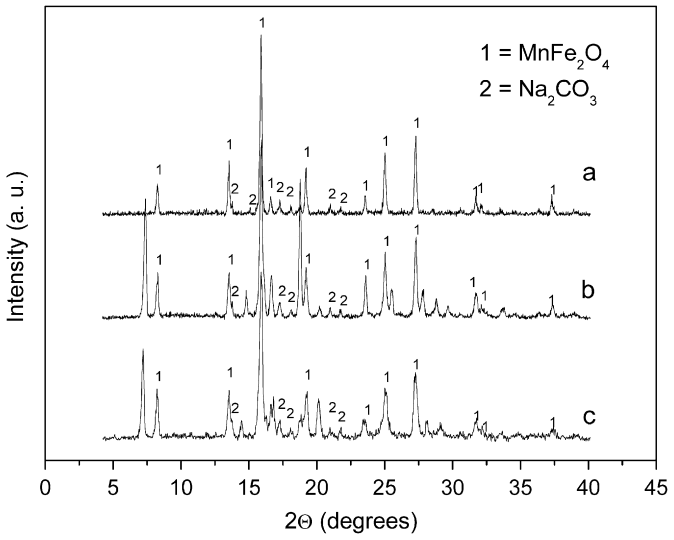

Fig. 3. XRD patterns representative of identified existence fields in the T/P_{CO_2} diagram. Curves a, b and c correspond to powders obtained in A, B and C existence fields. Identified phases are specified: (1) manganese ferrite and (2) sodium carbonate.

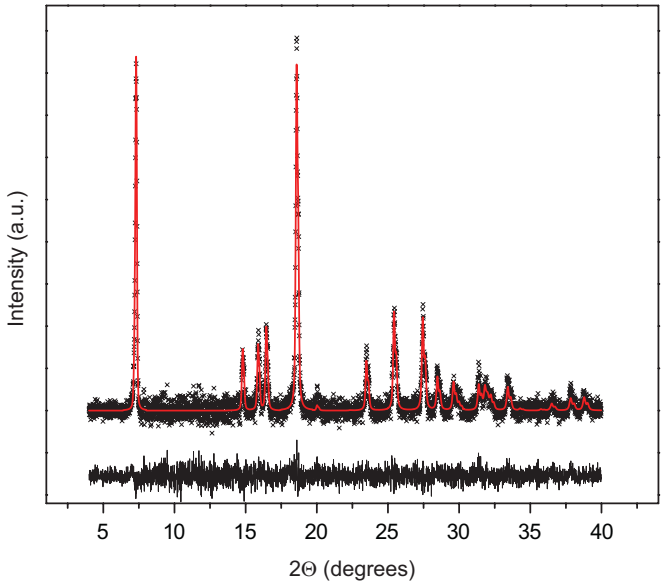

Fig. 4. XRD pattern of synthesized reference $Na(Mn_{1/3}Fe_{2/3})O_2$. Rietveld refinement ($R_{wp} = 4.44\%$) was performed using α-$NaFeO_2$ as the starting structural model.

3.2.1. The stoichiometric compound: the O3 phase

By analyzing crystallographic data, the stoichiometric $NaMn_{1/3}Fe_{2/3}O_2$ compound appears to be isostructural to α-$NaFeO_2$ phase, whose crystalline structure belongs to the $R\bar{3}m$ space group (SG). The observed phase belongs to a class of lamellar compounds widely utilized in rechargeable batteries [20,21], because of the high intra-lamellar mobility of the alkaline metal ion in the crystalline network. The oxygen environment of the alkali ion (O = octahedral, P = prismatic), followed by a number related to MO_2 (M = transition metal) sheets within the unit cell permits one to define a simple notation for this class of materials. α-$NaFeO_2$ is the prototype phase of O3 structures.

In Fig. 4 a graphical representation of the Rietveld analysis performed on the synthesized pure $Na(Mn_{1/3}Fe_{2/3})O_2$ reference compound is reported. α-$NaFeO_2$ O3 structure was utilized as a starting model. As evidenced by the low residual weighted pattern (R_{wp}) value (4.44%), the replacement of 1/3 of Fe^{III} ions by Mn^{III} is highly compatible with the hypothesized group symmetry.

3.2.2. The sub-stoichiometric compounds: the O3 and P3 phases

Fig. 5 reports a representative Rietveld analysis for powder samples coming from the B region. In the refinement, $MnFe_2O_4$ (SG $Fd\bar{3}m$) and Na_2CO_3 (SG $C12/m1$) starting models were added to the previously refined $Na(Mn_{1/3}Fe_{2/3})O_2$ phase. Fitted patterns revealed that, due to the prolonged exposure to CO_2, some sodium de-intercalation from $Na(Mn_{1/3}Fe_{2/3})O_2$ occurred. The obtained fit indexes, reported in Table 1, indicate that, at this stage, the lamellar O3 α-$NaFeO_2$-type structure is retained. The isolated numerical fitting of this phase is reported in the inset of Fig. 5 (B region) and its striking similarity to the pristine $Na(Mn_{1/3}Fe_{2/3})O_2$ O3 phase is evident. Sodium content in the compound was estimated at a value around 0.8 in all examined samples. To retain electroneutrality of the crystal structure, the Na sub-stoichiometry can be balanced either by a partial Mn^{III} to Mn^{IV} oxidation or by a limited O_2 release (δ) from the crystalline network, without significant changes in the pattern simulation. An experimental study on the early stage of the disproportion reaction is in course to define which one of the two hypothesized

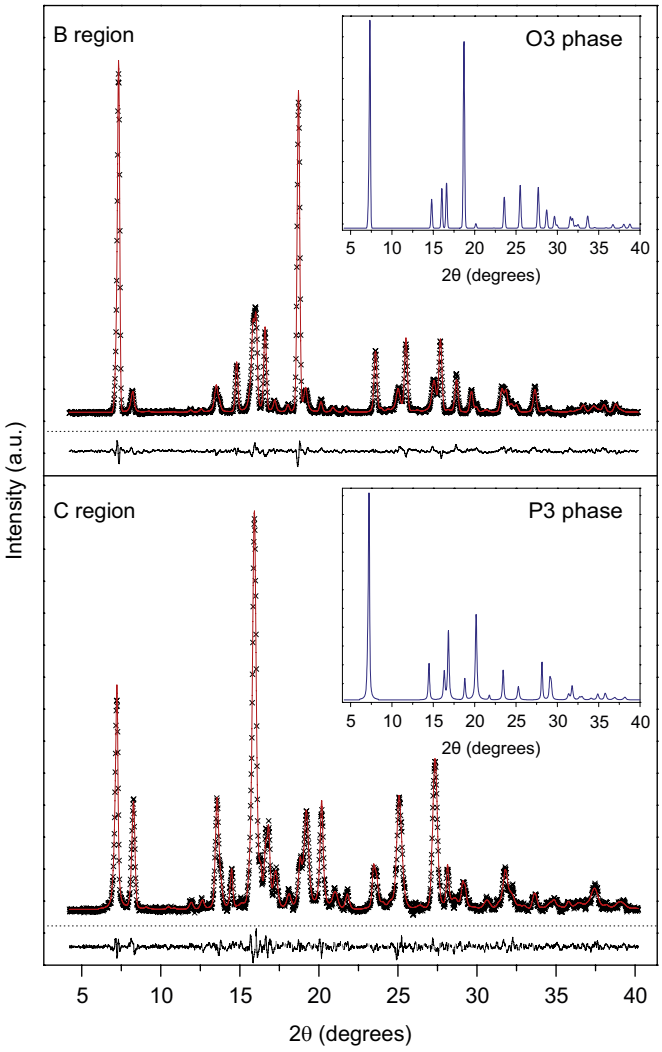

Fig. 5. XRD pattern and Rietveld refinement of two samples treated at $P_{CO_2} = 0.2$ atm, $T = 750\,^{\circ}C$ (B region, $R_{wp} = 8.83\%$) and $P_{CO_2} = 0.5$ atm, $T = 600\,^{\circ}C$ (C region, $R_{wp} = 11.56\%$). The numerical fitting relative only to the two sub-stoichiometric O3 and P3 phases, resulting from the Rietveld analysis, is reported in the inset.

Table 1
Rietveld quantitative phase analysis (weight %) performed on samples observed after different temperature/CO_2 pressure exposure

pCO_2 (atm)	T (°C)	Weight fraction (%)				Indexes of fit		
		$MnFe_2O_4$	Na_2CO_3	O3	P3	R_{wp} (%)	R_p (%)	χ^2
0.2	600	47.5(2)	33.2(1)		19.3(1)	11.27	9.34	2.102
	700	32.4(2)	28.4(8)	39.2(2)		9.99	8.30	1.593
	750	20.9(2)	16.9(5)	62.2(1)		8.83	6.91	1.565
	800	19.0(2)	13.0(5)	68.0(1)		9.67	7.62	2.110
0.5	600	47.2(2)	32.8(5)		20.0(2)	11.56	9.36	1.018
	700	58.0(1)	39.9(2)		2.1(4)	6.83	5.14	1.308
	750	57.9(1)	38.8(4)	3.3(1)		9.64	7.51	2.194
	800	35.6(1)	36.1(5)	28.3(1)		10.38	7.70	1.508
0.8	600	50.8(1)	32.3(4)		16.9(1)	9.97	7.89	1.554
	700	57.6(1)	39.5(4)		2.9(1)	10.61	8.17	1.697
	750	59.5(1)	40.5(6)			10.39	8.02	1.244
	800	60.2(2)	39.8(7)			9.03	7.63	1.086
1.0	600	51.6(1)	31.9(5)		16.5(2)	10.97	9.10	1.670
	700	60.0(2)	40.0(3)			9.69	7.91	1.404
	750							
	800	60.1(1)	39.9(3)			10.48	8.83	1.608

cases occurs. For the purpose of this work, it can be pointed out that the sub-stoichiometric sodium ferrimanganite observed in the B region of the T/P_{CO_2} diagram remains isostructural to the starting O3 $Na(Mn_{1/3}Fe_{2/3})O_2$ phase.

The XRD pattern of a sample belonging to the C region is also reported in Fig. 5 together with its Rietveld refinement. In the inset of the figure, the numerical fitting relative to the sub-stoichiometric sodium ferrimanganite, as resulting from Rietveld analysis, is reported. In this case the phase was assumed to be isostructural to the $Na_{0.60}CoO_2$ compound. This is a lamellar phase exhibiting a P3 structure and belonging to the SG $R3m$ [22–24]. The structure obtained by the Rietveld refinement is in agreement with a P3 sub-stoichiometric sodium ferrimanganite, with a roughly estimated sodium content of 0.6. Similarly to the case of the O3 phase, Na sub-stoichiometry can be either balanced by Mn^{III} to Mn^{IV} oxidation or by a partial O_2 release from the crystalline network without significant changes in pattern refinement. In the following we will refer to the compound as P3 phase.

3.2.3. Some crystallographic notes

In Table 2 Rietveld analysis results for O3 $Na(Mn_{1/3}Fe_{2/3})O_2$ stoichiometric compound are reported together with data relative to sub-stoichiometric compounds obtained by refinement of XRD patterns containing sodium-depleted ferrimanganites. Sub-stoichiometric O3 and P3 phases always appear in equilibrium with $MnFe_2O_4$ and Na_2CO_3; therefore data reported for these phases were obtained by analyzing patterns where contribution of the sub-stoichiometric phase was prevailing.

When compared to α-$NaFeO_2$ compound, the stoichiometric O3 $Na(Mn_{1/3}Fe_{2/3})O_2$ phase shows an elongation of the hexagonal unit cell along the c-axis (that increases from 16.09 Å, JCPDS card no. 20-1115, to 16.36 Å) due to partial Fe^{III} substitution with Mn^{III}. The observed elongation can be ascribed to the Jahn–Teller effect. In fact high-spin Mn^{III} in octahedral coordination is stabilized by a reticular distortion that induces, as a macroscopic effect, an increase of the c cell parameter and a shrinkage of the a parameter.

Sodium deficiency in the depleted $Na_{1-x}Mn_{1/3}Fe_{2/3}O_{2-\delta}$ O3 and P3 compounds promotes a further cell elongation, as a consequence of increased repulsive interactions between oxygen layers.

Table 2
Ferrimanganite lamellar phases involved in CO_2-induced $NaMn_{1/3}Fe_{2/3}O_2$ disproportion reaction

Nominal composition	Na coordination	Space group	$a=b$ (Å)	c (Å)	R_{wp} (%)
$Na(Mn_{1/3}Fe_{2/3})O_2$	O3	$R\bar{3}m$	2.983(1)	16.36(2)	4.44
$Na_{0.80}(Mn_{1/3}Fe_{2/3})O_{2-\delta}$	O3	$R\bar{3}m$	2.952(3)	16.46(4)	8.83[a]
$Na_{0.60}(Mn_{1/3}Fe_{2/3})O_{2-\delta}$	P3	$R3m$	2.919(3)	16.87(3)	11.56[a]

All phases exhibit a trigonal crystal lattice described by the hexagonal axes representation.
[a] Data obtained from the refinement of powder mixtures (see Table 1).

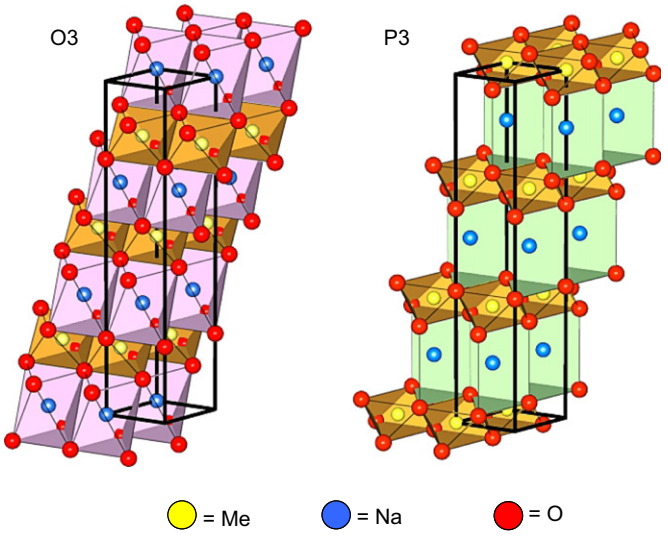

Fig. 6. Polyhedral representation of O3 and P3 layered structures. Unit cell is reported in bold.

A decrease in Na content from 1 to around 0.80 results in unit cell constant c increase from 16.36 to 16.46 Å, producing as well an increase in d_{003} and d_{104} interplanar spacing. As a consequence the reflections (003) and (104) in the stoichiometric compound, observed at $2\theta = 7.56°$ and $2\theta = 18.79°$ respectively (see Fig. 4), move to $2\theta = 7.38°$ and $2\theta = 18.70°$ in the sub-stoichiometric O3 compound (Fig. 5, B region).

In the P3 phase the (104) reflection almost disappears and the (003) reflection moves to $2\theta = 7.26°$ (Fig. 5, C region). In Fig. 6 the different sodium environments for O3 and P3 structures are reported.

Depending on the degree of sodium depletion, the lamellar $Na_{1-x}Mn_{1/3}Fe_{2/3}O_{2-\delta}$ compound may transform between the O3 and P3 phases. These transitions involve only a relative displacement of adjacent Me–O planes. Such structural transformations are not unusual for compounds that experience alkali ions extraction, in particular for sodium-containing lamellar compounds [22–26].

3.3. Regenerative step and chemical equilibria

Table 1 reports results of the Rietveld QPA performed on powder samples after thermal treatments. Obtained relative phase amounts allow one to calculate reaction yields by defining a reaction conversion degree (α) according to the following equation:

$$\alpha = (x_{wt}^{exp}/x_{wt}^{o})_{MnFe_2O_4} \quad (3)$$

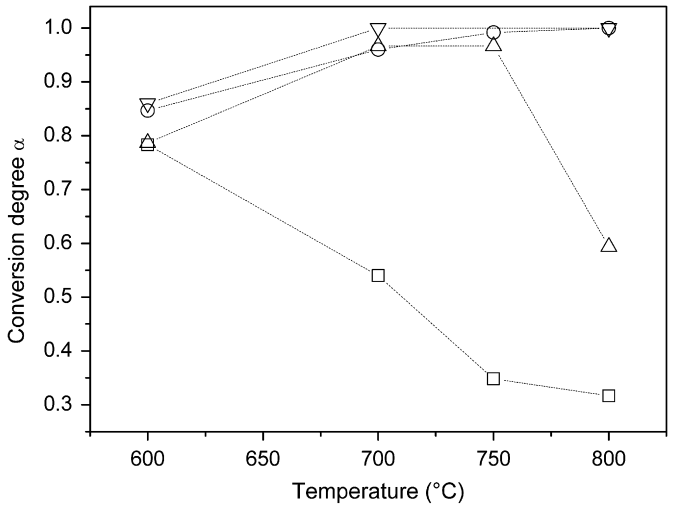

Fig. 7. Conversion degree α of reaction (2) as a function of temperature, calculated at different carbon dioxide pressures. $P_{CO_2} = 0.2$(--□--), 0.5 (--Δ--), 0.8 (--○--) and 1.0 (--∇--) atm.

where (x_{wt}^{exp}) and (x_{wt}^{o}) are the experimentally found and the theoretically expected (59.2%) values of manganese ferrite weight fraction in the mixture. A plot showing reaction yield vs. temperature is reported in Fig. 7. At 600 °C all reacted samples exhibit a conversion degree α falling in the 0.7–0.9 range. For higher temperatures, three different behaviors can be observed, depending on the CO_2 partial pressure. Samples processed at 1.0 and 0.8 atm show a raise in conversion degree at increasing temperature, reaching the expected theoretical value at 700 and 750 °C respectively. On the contrary, the samples reacted at 0.2 atm exhibit decreasing α values as temperature increases. Conversion values observed at 600 °C (~0.80 in both cases) decrease down to ~0.3 at 800 °C. Finally, samples processed at 0.5 atm show α values increasing from ~0.85 at 600 °C up to ~0.94 at 750 °C and then falling down to ~0.61 at 800 °C. The observed behavior is incompatible with the regenerative step described in reaction (2) and suggests further discussion.

Considering that the chemical transformation to restore the starting $MnFe_2O_4/Na_2CO_3$ mixture is actually reaction (2), the equilibrium constant (4) for the disproportion reaction (K_{disp}) can be defined:

$$K_{disp} = \frac{a^2_{MnFe_2O_{4(s)}} a^3_{Na_2CO_{3(s)}} a^{1/2}_{O_{2g}}}{a^6_{NaMn_{1/3}Fe_{2/3}O_{2(s)}} a^3_{CO_{2g}}} \quad (4)$$

where the a_i term represents the chemical activity of the i compound in the reacting system. Representing activities of gaseous species in terms of their pressure (fugacity of gases can be reasonably approximated by their pressure in the present view), Eq. (4) becomes the following:

$$K_{disp} = \frac{a^2_{MnFe_2O_{4(s)}} a^3_{Na_2CO_{3(s)}} p^{1/2}_{O_2}}{a^6_{NaMn_{1/3}Fe_{2/3}O_{2(s)}} p^3_{CO_2}} \quad (5)$$

Naturally, at a given temperature and considering as unitary the activities of solids, the $p^{1/2}_{O_2}/p^3_{CO_2}$ ratio defines the equilibrium constant of reaction (2) when a closed system is considered. In practical terms, a $Na(Mn_{1/3}Fe_{2/3})O_2$, $MnFe_2O_4$ and Na_2CO_3 mixture releases CO_2 and O_2 till it reaches $p^{1/2}_{O_{2(g)}}/p^3_{CO_{2(g)}} = K_p$ when placed in a isothermal reactor that does not exchange matter with the external environment. In this work all experiments were conducted in Ar/CO_2 gaseous flux and for a reaction time long enough to have a complete transformation or a stationary reaction yield, as verified by constant weight gain in thermogravimetric curves. The utilized gaseous flux condition corresponds to an open system, where a continuous introduction of CO_2 and extraction of O_2 from reaction chamber is performed. Continuous O_2 removal from the reactor should promote the transformation of all solid phases into a $MnFe_2O_4/Na_2CO_3$ mixture for all imposed reaction conditions. Contrary to prediction, this behavior was not observed and several equilibrium compositions corresponding to coexistence between sodium-depleted compounds, sodium carbonate and manganese ferrite (see Table 1) were observed. This can occur only if Eq. (2) is the result of a series of different chemical reactions, as given in the following equations:

$$NaMn_{1/3}Fe_{2/3}O_{2(s)} + \frac{x}{2}CO_{2(g)} \rightleftharpoons \frac{x}{2}Na_2CO_{3(s)} + Na_{1-x}Mn_{1/3}Fe_{2/3}O_{2-\delta(s,O3/P3)} \quad (6)$$

$$Na_{1-x}Mn_{1/3}Fe_{2/3}O_{2-\delta(s,O3/P3)} \rightleftharpoons \frac{1}{3}MnFe_2O_{4(s)} + \frac{1-x}{2}Na_2O_{(s)} + yO_{2(g)} \quad (7)$$

$$\frac{1-x}{2}Na_2O_{(s)} + \frac{1-x}{2}CO_{2(g)} \rightleftharpoons \frac{1-x}{2}Na_2CO_{3(s)} \quad (8)$$

where x is the amount of sodium extracted from the lamellar phase in the given experimental conditions (T, p) and $y \leqslant 1/2 (= 1/2$ for complete Mn^{III} to Mn^{II} transformation).

The $MnFe_2O_4$ restoring reaction begins with diffusion of sodium ions toward grain boundaries of sodium manganese ferrite particles, induced by reaction with CO_2 to form Na_2CO_3. A sub-stoichiometric sodium ferrimanganite is the product of this first transformation. The sodium-depleted ferrimanganite can organize the crystalline network in either O3 or P3 forms, depending on its sodium content. When the sodium content becomes too low to preserve the lattice stability, the sodium ferrite network irreversibly collapses expelling oxygen (fluxed out) (reaction (7)), producing the manganese spinel phase and free Na_2O, which immediately reacts with carbon dioxide to produce additional Na_2CO_3 (reaction (8)). According to this multi-step mechanism, $MnFe_2O_4$ regeneration is governed by the sodium depletion in the starting ferrimanganite, therefore reaction (7) should control the overall equilibrium of the transformation. Since reaction (6) is sensitive to CO_2 pressure and insensitive to O_2 content, it cannot be forced to completion by simply taking away oxygen gas from the reactor, and equilibrium values of transformation degree α falling in the 0–1 range can be observed.

Na_2CO_3 formation/dissociation equilibrium also plays an important role in the reaction sequence. From thermodynamic calculations [27] it can be easily observed that the degree of Na_2CO_3 dissociation increases at increasing temperatures and at low CO_2 pressure values. When the reactive system is treated at temperature and pressure conditions so as to have discrete quantities of free Na_2O at the $Na_{1-x}(Mn_{1/3}Fe_{2/3})O_{2-\delta}/Na_2CO_3$ interface as a result of carbonate dissociation (reaction (8) equilibrium is shifted to the left), further sodium depletion is inhibited and, as a consequence, a lower $MnFe_2O_4$ transformation degree is observed. The mechanism fits well with the observation reported in Fig. 7. At low CO_2 pressure values (0.2 atm in the figure), any temperature increase enhances the dissociation of sodium carbonate. As a consequence, lower sodium depletion occurs and the overall $Na(Mn_{1/3}Fe_{2/3})O_2$ to $MnFe_2O_4$ transformation degree decreases. At 0.5 atm, CO_2 pressure slightly inhibits Na_2CO_3 dissociation, and regression in reaction (7) is observed for temperatures higher than 750 °C. Higher experimental CO_2 pressure values (0.8 and 1 atm) shift by mass effect reaction (8) toward sodium carbonate formation also at higher temperatures. Sodium carbonate formation, depleting the mixed ferrite

from sodium, favors the structural rearrangement associated with oxygen evolution (reaction (7)). Work is in progress to determine if both O3 and P3 phases can collapse into manganese ferrite expelling sodium oxide.

4. Conclusions

Reversibility conditions of the manganese ferrite water-splitting cycle were investigated performing sodium ferrimanganite disproportion reaction at low (0.2–1.0 atm) carbon dioxide pressure in the temperature range $600<T<800\,^{\circ}C$. Reacted powders were analyzed by using the XRD technique and Rietveld analysis performed on collected data. Analysis of XRD patterns allowed defining a region in T/P_{CO_2} diagram where manganese ferrite and sodium carbonate are fully regenerated. Depending on reaction conditions, phases different from the expected sodium carbonate and manganese ferrite are observed. These phases are layered compounds whose structure was determined by Rietveld refinement. These intermediate compounds consist of two different Na sub-stoichiometric ferrimanganite phases $Na_{1-x}(Mn_{1/3}Fe_{2/3})O_{2-\delta}$ having O3 and P3 lamellar crystalline structures.

Based on experimental observations, a multiple-step mechanism is proposed for the disproportion reaction. Sodium de-intercalation from lamellar compounds and sodium carbonate stability equilibria play a significant role in determining the final products' composition. Sodium depletion and oxygen release from the crystalline network of lamellar compounds can be forced by means of carbon dioxide that leads sodium carbonate formation to completion.

Acknowledgment

This work was financed by the Italian Ministry of Research by means of the TEPSI project.

References

[1] Y. Tamaura, Y. Ueda, J. Matsunami, N. Hasegawa, M. Nezuka, T. Sano, M. Tsuji, Sol. Energy 65 (1999) 55–57.
[2] H. Kaneko, Y. Ochiai, K. Shimizu, Y. Hosokawa, N. Gokon, Y. Tamaura, Sol. Energy 72 (2002) 377–383.
[3] C. Alvani, A. La Barbera, G. Ennas, F. Padella, F. Varsano, Int. J. Hydrogen Energy 31 (2006) 2217–2222.
[4] J.E. Funk, Int. J. Hydrogen Energy 26 (2001) 185–190.
[5] A. Steinfeld, Sol. Energy 78 (2005) 603–615.
[6] T. Nakamura, Sol. Energy 19 (1977) 467–475.
[7] M. Lundberg, Int. J. Hydrogen Energy 18 (1993) 369–376.
[8] C. Agrafiotis, M. Roeb, A.G. Kostandopoulos, L. Nalbandian, V.T. Zaspalis, C. Sattler, P. Stobbe, A.M. Steele, Sol. Energy 79 (2005) 409–421.
[9] Solar hydrogen generation project 〈http://shgr.unlv.edu〉.
[10] F. Padella, C. Alvani, A. La Barbera, G. Ennas, R. Liberatore, F. Varsano, Mater. Chem. Phys. 90 (2005) 172–177.
[11] C. Alvani, A. La Barbera, G. Ennas, F. Padella, F. Varsano, Int. J. Hydrogen Energy 30 (2005) 1407–1411.
[12] L. Seralessandri, F. Varsano, A. La Barbera, F. Padella, Scr. Mater. 55 (2006) 875–877.
[13] H. Kaneko, Y. Hosokawa, N. Gokon, N. Kojima N, N. Hasegawa, M. Kitamura, Y. Tamaura, J. Phys. Chem. Solids 62 (2001) 1341–1347.
[14] H. Kaneko, Y. Hosokawa, N. Kojima, N. Gokon, N. Hasegawa, M. Kitamura, Y. Tamaura, Energy 26 (2001) 919–929.
[15] PCPDF-WIN Version 2.01, November 1998 ICPDS.ICDD.
[16] H.M. Rietveld, J. Appl. Crystallogr. 22 (1969) 65–71.
[17] R.A. Young, The Rietveld Method, IUCr Monographs on Crystallography 5, Oxford University Press, 1993.
[18] A.C. Larson, R.B. Von Dreele, General Structure Analysis System (GSAS), Los Alamos National Laboratory Report LAUR 86-748, 2004.
[19] ICSD—Inorganic Crystal Structure Database version 2004-02.
[20] C. Delmas, C. Fouassier, P. Hagenmuller, Physica B&C 99 (1980) 81–85.
[21] T.A. Eriksson, Y.J. Lee, J. Hollingsworth, J.A. Reimer, E.J. Cairns, X. Zhang, M.M. Doeff, Chem. Mater. 15 (2003) 4456–4463.
[22] C. Fouassier, G. Matejka, J. Reau, P. Hagenmuller, J. Solid State Chem. 6 (1973) 532–537.
[23] M. Mikami, M. Yoshimura, Y. Mori, T. Sasaki, R. Funahashi, I. Matsubara, Jpn. J. Appl. Phys. 41 (2002) L777–L779.
[24] I. Saadoune, A. Maazaz, M. Ménétrier, C. Delmas, J. Solid State Chem. 122 (1996) 111–117.
[25] A. Mendiboure, C. Delmas, P. Haegenmuller, J. Solid State Chem. 57 (1985) 323–331.
[26] M.C. Blesa, E. Moran, C. Leòn, J. Santamaria, J.D. Tornero, N. Menéndez, Solid State Ionics 126 (1999) 81–87.
[27] A. Roine, HSC Chemistry 5.11, Outokumpu Research Oy, Pori, Finland, 2002.